Propagation and focusing characteristics of the Bessel–Gaussian beam with the spiral phase term of new power-exponent-phase

Aotian Wang(王傲天)[1,2], Lianghong Yu(於亮红)[1,†], Jinfeng Li(李进峰)[1], and Xiaoyan Liang(梁晓燕)[1,‡]

[1] *State Key Laboratory of High Field Laser Physics, Shanghai Institute of Optics and Fine Mechanics, Chinese Academy of Sciences, Shanghai* 201800, *China*
[2] *Center of Materials Science and Optoelectronics Engineering, University of Chinese Academy of Sciences, Beijing* 100049, *China*

(Received 14 November 2022; revised manuscript received 30 December 2022; accepted manuscript online 11 January 2023)

A new type of beam called the NPEP-BG (a Bessel–Gaussian (BG) beam with a spiral phase term of a new power-exponent-phase (NPEP)) is theoretically studied in this paper. The results show that the number of singularities of the phase and side lobes of the intensity of this beam were equal to the topological charges (TCs) and the beam has the characteristics of self-healing during propagation. The NPEP-BG beam combined the partial characteristics of the new power-exponent-phase vortex (NPEPV) and the Bessel–Gaussian beam. At the focus of the beam, the characteristic like a perfect vortex beam was present, in which the focal radius is stable and independent of the topological charge. There are multi-focal spots around a ring in the focal plane, meaning that the NPEP-BG beam has a potential for application in multi-particle manipulation.

Keywords: vortex, new-power-exponential-phase, Bessel–Gaussian beam, focus

PACS: 42.25.Bs **DOI:** 10.1088/1674-1056/acb1fe

1. Introduction

Since Allen generated a Laguerre–Gaussian (LG) vortex beam using mode converts and proved that vortex beams have orbital angular momentum (OAM) in 1992,[1] various types of vortex beams have been generated and studied by researchers. Vortex beams have been widely used in many fields such as optical communications,[2–4] super-resolution fluorescence microscopy,[5] optical tweezers,[6] and particle acceleration.[7] In addition to the common LG vortex beam,[1] other vortex beams have been studied, such as the fractional vortex,[8] high-order Bessel beam,[9] and perfect vortex (PV).[10–12]

Recently, new vortex beams (those different from previous vortex beams) have been studied, such as the power-exponent-phase vortex (PEPV),[13] the remainder phase vortex,[14] and a combination of both called the new PEPV (NPEPV).[15] These vortex beams have a power exponent phase term, that is $\exp(\mathrm{i}2l\pi(\theta/2\pi)^n)$ for PEPV and $\exp(\mathrm{i}2\pi(rem(l\theta,2\pi)/2\pi)^n)$ for NPEPV, which is different from $\exp(\mathrm{i}l\theta)$ for LG, where the l index associated with the OAM, and the n index is the power order of the beam. The number of phase singularities and side lobes is equal to the topological charges (TCs) for the PEPV and NPEPV beams, and there is more than one phase singularity if the TC is higher than 1. The phase singularities and side lobes were symmetrically distributed around the central axis of the beams. PEPV has been applied to multi-particle manipulation.[16]

The ideal Bessel beam is a non-diffraction beam.[17,18] However, researchers can only generate Bessel-like beams in experiments, such as Bessel–Gaussian (BG) beams, and it is impossible to generate an ideal Bessel beam because its optical field has infinite energy. Durnin *et al.* (1987) [19] generated a BG with a Gaussian beam passing through an annular slit and lens. The general methods for generating BG beams include a axicon which a beam pass through,[20] a spatial light modulator (SLM) loading with a corresponding phase mask to a beam,[21] *etc.* Owing to their non-diffraction properties and long depth of focus, BG beams have been applied in optical communications,[22] material processing,[23] and optical trapping, *etc.*[23]

A perfect vortex (PV) beam can be generated at the focal point by a BG beam passing through a convex lens.[11] Contrary to the common vortex like LG beam, in which the radius of ring-like transverse intensity profile scales up to the TCs, PV has fixed radius of ring transverse which is independent of TCs.[11] Compared with LG beams with the same OAM, PVs can propagate in smaller core diameter fibers and have greater potential for application in optical communications[3] and particle manipulation.[12]

In this study, we investigated the characteristics of a new type of beam called the NPEP-BG beam, which is a Bessel–Gaussian (BG) beam with a spiral phase term of a new power-exponent-phase (NPEP) of $\exp(\mathrm{i}2\pi(rem(l\theta,2\pi)/2\pi)^n)$. The characteristics of this beam demonstrate not only the characteristics of the NPEPV[15] during the propagation, but also the characteristics of a Bessel–Gaussian beam, such as self-healing. The focus has perfect vortex optical characteristics as a Bessel beam, and it has important application prospects in multi-particle manipulation.

†Corresponding author. E-mail: lhyu@siom.ac.cn
‡Corresponding author. E-mail: liangxy@siom.ac.cn

© 2023 Chinese Physical Society and IOP Publishing Ltd

2. Propagation formula of NPEP-BG beam

NPEP-BG is defined as a BG beam with a spiral phase term of a new power-exponent phase. Therefore, the electric field form of the light source plane is as follows:

$$E(r,\theta) = A_0 \mathrm{J}_l(k_r r)\exp\left(-\frac{r^2}{\omega_0^2}\right) \times \exp\left\{\mathrm{i}2\pi\left[\frac{rem(l\theta,2\pi)}{2\pi}\right]^n\right\}, \tag{1}$$

where r, θ are the polar coordinates, l is the TC or Bessel function's order number, n is the power order, ω_0 is the Gaussian beam waist, $\mathrm{J}_l(x)$ is the l-order Bessel function, and k_r is the radial wave number ($k_r = 2.405/r_0 = 2\pi\sin\varphi/\lambda$). r_0 is the location of the first zero point of the first kind of zero-order Bessel function at the positive x axis for $\mathrm{J}_l(k_r x)$, or the radius of the central lobe of the first kind of zero-order Bessel function, φ is the angle between the wave vector and propagation direction, and we use ρ_0 to represent $\lambda/\sin\varphi$. A is the amplitude of NPEP-BG beam electric field. The phase term of $\exp(\mathrm{i}l\theta)$ of the BG beam, is replaced by the NPEP term of $\exp(\mathrm{i}2\pi(rem(l\theta,2\pi)/2\pi)^n)$.

Fresnel diffraction integration is used to derive the expression of the electric field distribution of the NPEP-BG beam propagating in polar coordinates. The Fresnel diffraction integral formula in polar coordinates (Eq. (2))[11] is as follows:

$$E(\rho,\phi,z) = \frac{k}{\mathrm{i}2\pi z}\int_0^{2\pi}\int_0^{\infty} E(r,\theta)\exp\left[\frac{\mathrm{i}k}{2z}\left(\rho^2+r^2-2\rho r\cos(\theta-\phi)\right)\right] r\,\mathrm{d}r\,\mathrm{d}\theta. \tag{2}$$

According to Refs. [11,15] and Eq. (1), the spatial analytical expression of the electric field after the NPEP-BG beam propagates to the z distance is as follows:

$$\begin{aligned} E(\rho,\phi,z) = {} & \frac{k}{\mathrm{i}2\pi z}\exp\left(\frac{\mathrm{i}k}{2z}\rho^2\right)\exp(\mathrm{i}kz)\left\{\frac{M_0 k_r^l\left(\frac{1}{\omega^2}+\frac{\mathrm{i}k}{2z}\right)^{-(l+2)/2}}{2^{l+2}}\sum_{h=0}^{\infty}\frac{\Gamma\left(h+\frac{l}{2}+1\right)}{h!\Gamma(h+l+1)}\left(-\frac{k_r^2}{4\left(\frac{1}{\omega^2}+\frac{\mathrm{i}k}{2z}\right)}\right)^h\right. \\ & \times \mathrm{F}\left(-h,-l-h;1;\frac{k^2\rho^2}{z^2k_r^2}\right) + \sum_{m=1}^{\infty}\frac{(-\mathrm{i})^m k_r^l\left(\left(\frac{1}{\omega^2}+\frac{\mathrm{i}k}{2z}\right)^{-(l+m+2)/2}\right)}{2^{l+m+1}\Gamma(m+1)}\sum_{g=0}^{\infty}\frac{\Gamma\left(g+\frac{l+m}{2}+1\right)}{g!\Gamma(g+l+1)}\left(-\frac{k_r^2}{4\left(\frac{1}{\omega^2}+\frac{\mathrm{i}k}{2z}\right)}\right)^g \\ & \left.\times \mathrm{F}\left(-g,-l-g;m+1;\frac{k^2\rho^2}{z^2k_r^2}\right)\left(\mathrm{e}^{-\mathrm{i}m\phi}M_m+\mathrm{e}^{\mathrm{i}m\phi}M_{-m}\right)\right\}, \\ M_m = {} & \int_0^{2\pi}\exp\left\{\mathrm{i}2\pi\left[\frac{rem(l\theta,2\pi)}{2\pi}\right]^n+\mathrm{i}m\theta\right\}\mathrm{d}\theta = \begin{cases}\displaystyle\sum_{j=0}^{\infty}\sum_{p=0}^{\infty}\sum_{q=0}^{l-1}\frac{\mathrm{i}^{j+p}l^p(2\pi)^{j+p+1}\exp\left\{\mathrm{i}qm\left(\frac{2\pi}{m}\right)\right\}}{j!p!l^{p+1}(nj+p+1)}, & l\neq 0, \\ \displaystyle\sum_{j=0}^{\infty}\frac{\mathrm{i}^j(2\pi)^{j+1}}{j!(nj+1)}, & l=0, \end{cases} \end{aligned} \tag{3}$$

where $\Gamma(x)$ is the Gamma function, $\mathrm{F}(\alpha_1,\beta_1;\gamma_1;\zeta)$ is the hypergeometric function.

$$\mathrm{F}(\alpha_1,\beta_1;\gamma_1;\zeta) = 1+\frac{\alpha_1\beta_1}{\gamma_1}\zeta+\frac{\alpha_1(\alpha_1+1)\beta_1(\beta_1+1)}{\gamma_1(\gamma_1+1)2!}\zeta^2 + \frac{\alpha_1(\alpha_1+1)(\alpha_1+2)\beta_1(\beta_1+1)(\beta_1+2)}{\gamma_1(\gamma_1+1)(\gamma_1+2)3!}\zeta^3+\cdots.$$

3. Simulation

In the following chapters, the properties of non-diffraction, self-healing, and their phase distributions in the free-space propagation of NPEP-BG beams are studied theoretically using the electric field expression shown in Eq. (1) by the method of angular spectrum method. The parameters in this article are set as follows, $\rho_0 = 0.4$ mm, wavelength of $\lambda = 800$ nm, Gaussian beam waist of $\omega_0 = 1$ mm.

The NPEP-BG beam is a new type beam which combined the Bessel beam and the NPEPV beam. For better understanding, the phase distributions of NPEPV beam, BG beam, and NPEP-BG beam ($l = 2, n = 3$) were shown in Fig. 1 firstly. It can be seen that the phase distribution of NPEP-BG beam with $l = 2$ and $l = 3$ is similar to that of BG beam with $l = 2$. Both of them are composed of 0–2π annular-banded phase distribution. In each annular phase band of BG beam, the phase increases linearly with azimuth from 0 to 2π. While for the NPEP-BG beam, the phase of even-number annular bands increases exponentially with azimuth and the phase of odd-number annular bands increases in negative exponentially with azimuth. Compared the vertical intersection of two lines of 0–2π boundary for BG beam, the intersection angle of NPEP-BG beam changes slightly.

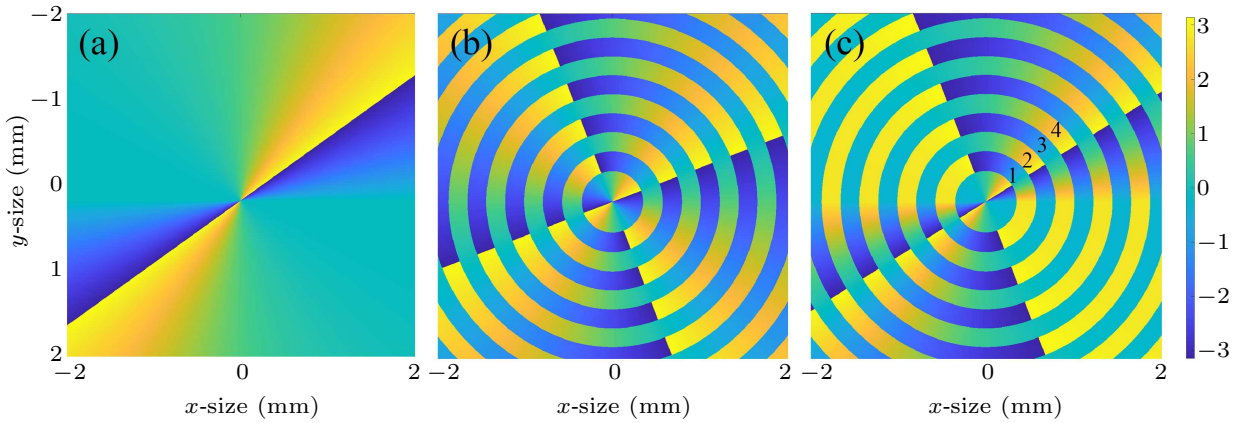


Fig. 1. (a) The phase distribution of NPEPV beam ($l = 2$, $n = 3$), (b) the phase distribution of BG beam ($l = 2$), (c) the phase distribution of NPEP-BG beam ($l = 2$, $n = 3$).

3.1. Propagation and cross sections at different distances

At source plane ($z = 0$) of NPEP-BG beams, its intensity distributions are the same as BG beams, and it changes with propagation distances. First, we studied the propagation characteristics of NPEP-BG beams. The intensity evolution in the direction of propagation (propagation distance of z from 0 m to 1 m) with different TCs (number of l) and the power exponent (number of n) are shown in Figs. 2(a0)–2(d0). The intensity is concentrated to a thin and long beam at the center of the x axis with the increase of propagation distance, and then diverged to a beam like a swallow's tail. This process of axial spike sustains a distance, and the distance changes with different TCs. The concentrated intensity is increased with n. The transverse intensity distributions at different distances ($z = 0.1$ m, 0.3 m, 0.5 m, and 0.7 m) in Figs. 2(a0)–2(d0) are shown in Figs. 2(a1)–2(a4), 2(b1)–2(b4), 2(c1)–2(c4), 2(d1)–2(d4). The transverse distributions were shown the rotation characteristics of central symmetry. The transverse intensity evolution with different l and n was studied in the following part.

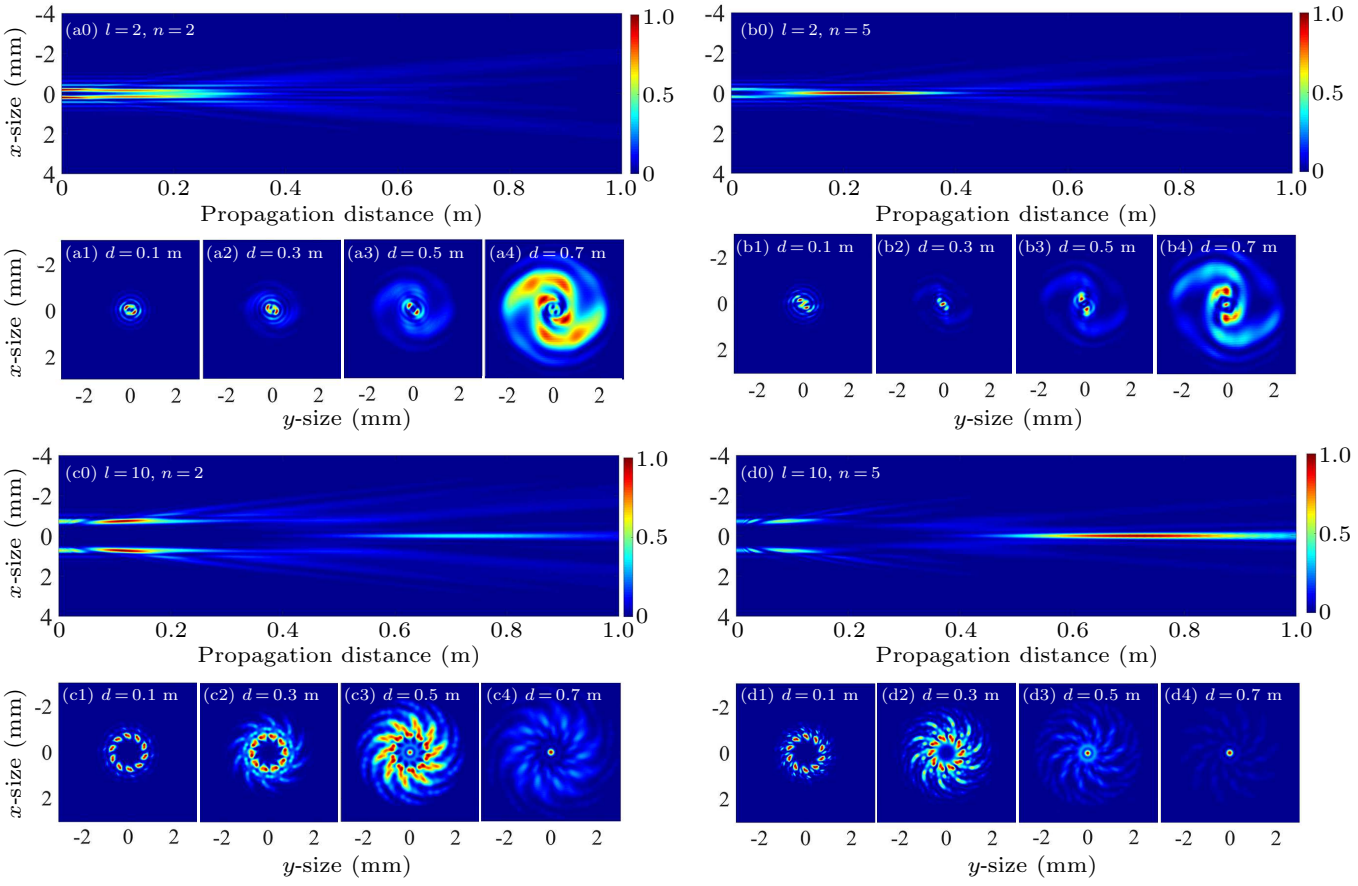


Fig. 2. Intensities (in units of arb. units) of NPEP-BG beam with different TCs (l) and power orders (n) on x–z plane [(a0)–(d0)] during the propagation process (z ranging from 0 m to 1 m). The transverse intensity distribution of NPEP-BG at different propagation distances with $z = 0$ m, 0.1 m, 0.5 m, and 0.5 m are shown in panels (a1)–(a4), (b1)–(b4), (c1)–(c4), and (d1)–(d4), respectively.

3.2. Change of NPEP-BG optical field cross sections with TCs and power orders

As shown in Fig. 3, different transverse intensity distributions were shown for different TCs and power orders. In this part, the transverse intensity distributions for different n and different l were studied respectively when $z = 0.2$ m, because this position can better show the characteristics of the beam as shown in Figs. 2(a0)–2(d0). Figure 3 shows the intensity and phase distributions of the NPEP-BG beam with different TCs of $l = 2$, 5, 10, 15 but the same power order $n = 2$. There are some ring-shaped intensity distributions surround the hollow center. The number of side lobe beams in the strongest ring is equal to their TCs, which is similar to the NPEPV beam. The intensity of each side spot beam is the same and the tail of each side spot shows rotation characteristics.

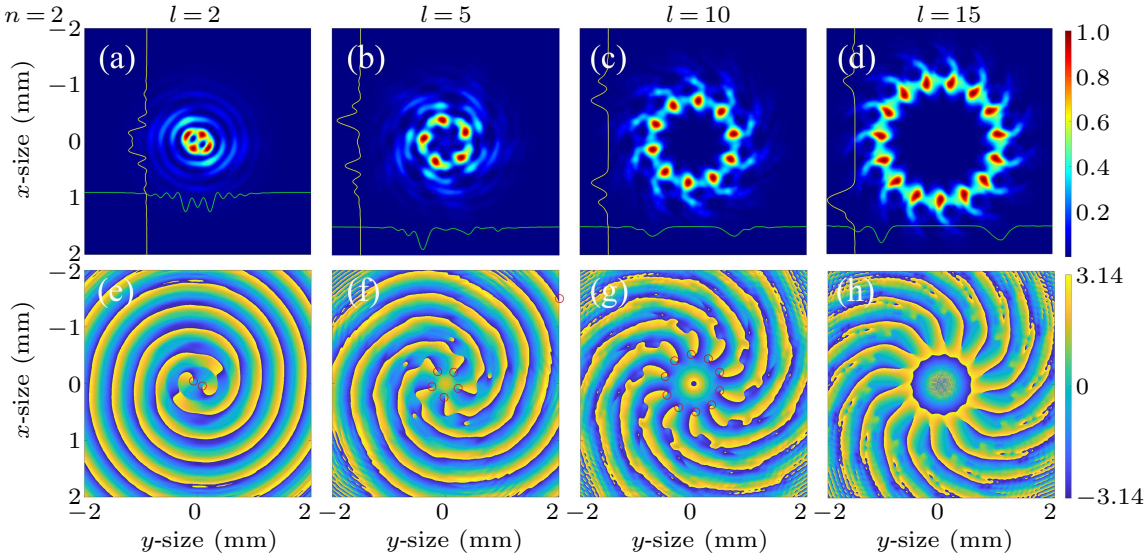


Fig. 3. (a)–(d) The intensity distributions, (e)–(h) the phase distributions for $l = 2$, 5, 10, 15, respectively, when $n = 2$.

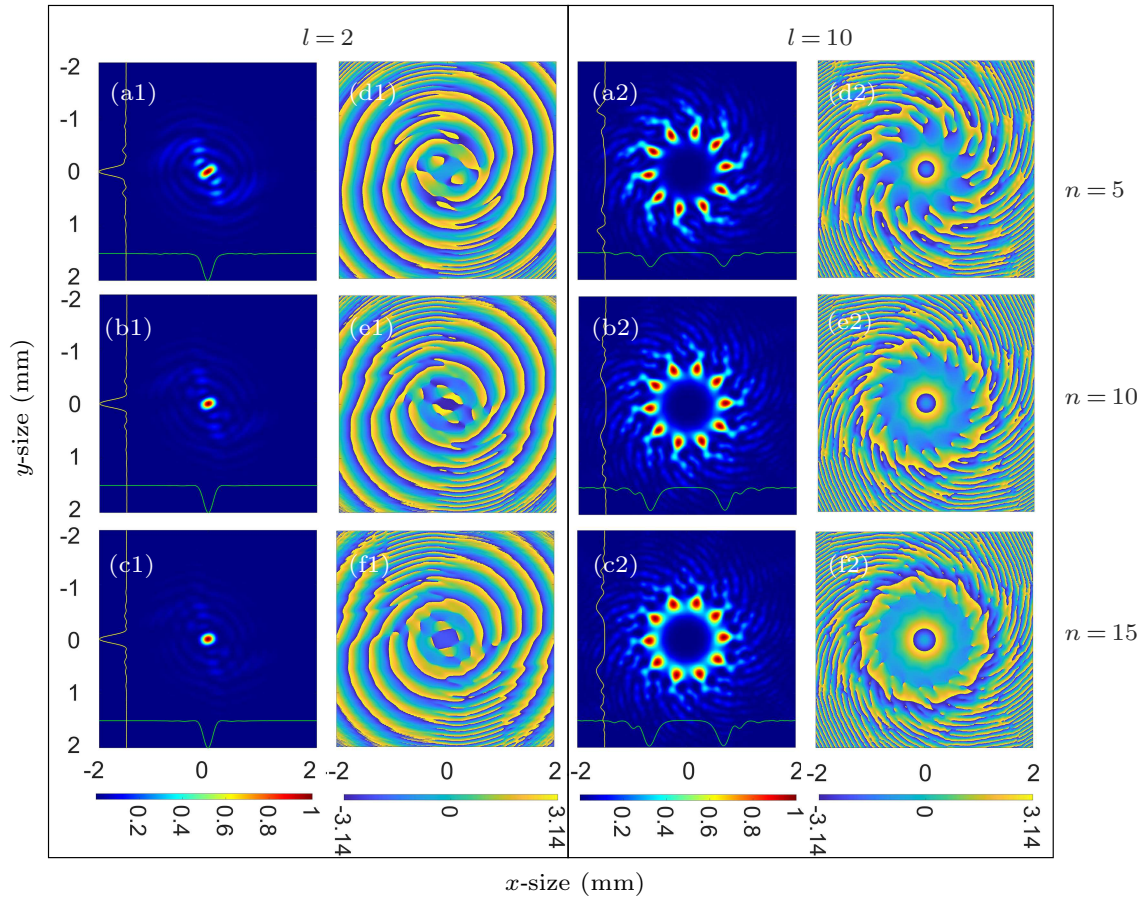


Fig. 4. (a1)–(c1) The intensity distributions and (d1)–(f1) the phase distributions for $n = 5, 10, 15$ respectively when $l = 2$; (a2)–(c2) the intensity distributions and (d2)–(f2) the phase distributions for $n = 5$, 10, 15, respectively, when $l = 10$.

Phase distributions are periodic around center of phase map in Figs. 3 and 4, and the number of periods is equal to TCs, which is also a property of conventional vortex beams. The places of phase singularities have been marked by red rings in Figs. 3(e)–3(g). It can be seen that when $l = 2$, 5, and 10, the phase singularities surround the center of phase map, and the distance between phase singularities and phase center increases with the increase of TCs. However, when $l = 15$, the phase singularities cannot be distinguished clearly in Fig. 3(h). The reason is that the phases of adjacent periods overlap near the center of phase map when TC is large, and the real places of phase singularities may be covered.

The intensity and phase distributions change with different l when $n = 2$ (Figs. 4(a1)–(f1)) and $n = 10$ (Figs. 4(a2)–(f2)), respectively, are shown in Fig. 4. For $l = 2$, the beam is concentrated to one spot at $z = 0.2$ m, and the intensity in center spot is increased with the increase of n. For $l = 10$, the number of side lobes in the strongest ring is equal to l and independent of n. The lobes in the ring closest to the center, which is the strongest ring, is also increased with the increase of n. Meanwhile, at $n = 2$, the phase distributions of the NPEP-BG beam are similar to those of the BG beams for different values of l (Fig. 3). However, the phase distributions of large TCs and power orders (Figs. 4(d2)–(f2)) are dissimilar to those of the BG beams (the phase distribution of high-order BG beams can be found in Ref. [22]). Furthermore, as the power order increased, the phase distributions of the NPEP-BG further deviated from those of the BG beams.

Interference is a typical method for measuring vortex beams.[11,24] Figure 5 shows the interference results of the NPEP-BG with a Gaussian beam. The interference patterns exhibit the typical characteristics of vortex beam interference with Gaussian beams. This interference pattern can obviously show the number of TCs, but not the power exponent. The power exponent can affect the distribution of interference pattern for same value of l.

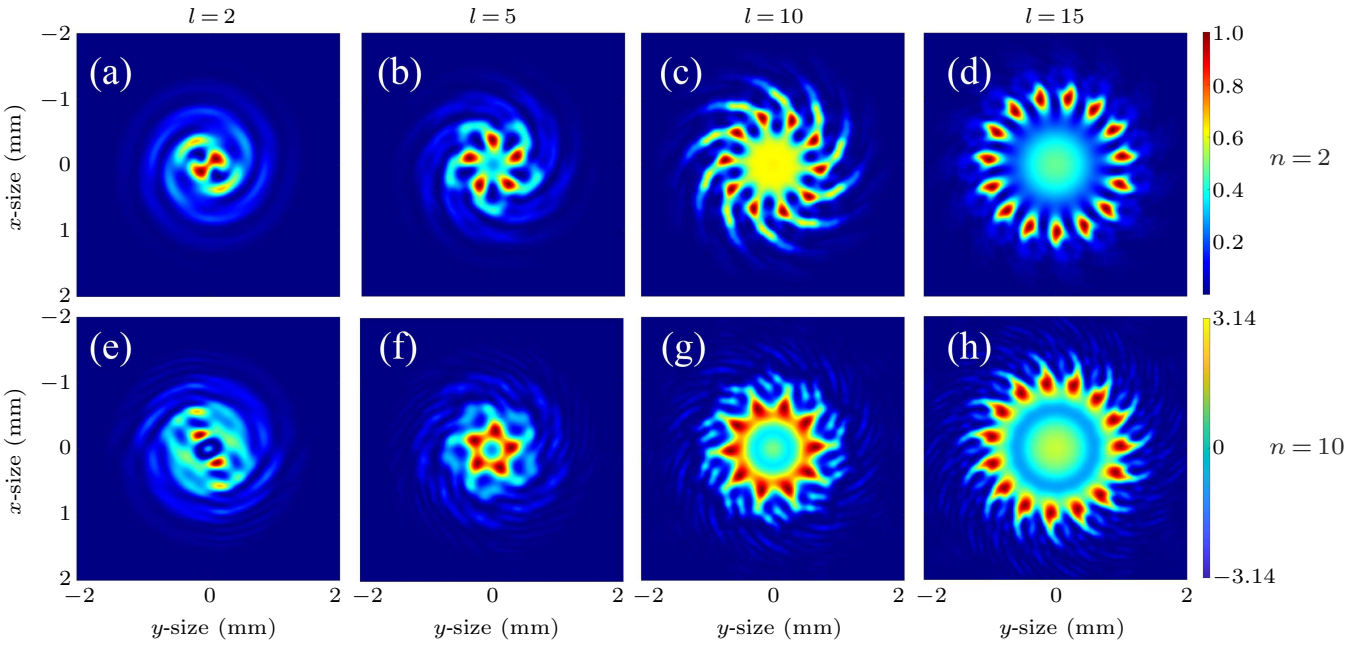


Fig. 5. Interference patters of NPEP-BG and Gaussian beams.

3.3. Self-healing of the NPEP-BG

Self-healing[23] is an important property of non-diffraction beams. These beams can recover after passing through an obstacle for a certain distance. The self-healing of the NPEP-BG beam was simulated as shown in Fig. 6, with a propagation distance ranging from 0 m to 3 m. Herein, to obtain a long propagation distance, we change the values of ρ_0 and ω_0 to $\rho_0 = 0.8$ mm and $\omega_0 = 5$ mm. The assignment of these parameters was only used in this part. A rectangular obstacle (0.6 mm × 6 mm) with no thickness was placed in the area surrounded by the green line in Figs. 6(g0) and 6(g1), where the distance was at $z = 0.5$ m.

For comparison with the NPEP-BG beam, the intensity evolution of the NPEPV beam propagating at different distances with and without obstacles is shown in Figs. 6(a0)–6(f0) in the first row and Figs. 6(g0)–6(l0) in the second row, respectively. It can be seen from the first and second rows that the intensity distributions with obstacles are very different from those without obstacles during propagation, which implies that NPEPV does not have the property of self-healing. The intensity evolution of NPEP-BG is shown in Figs. 6(a1)–6(f1) without obstacles and in Figs. 6(g1)–6(l1) with obstacles. Although the initial beam is partially blocked by obstacles, as shown in Fig. 6(g1), after propagating over a distance, the beam slowly self-heals into the similar shape as the unobstructed beam.

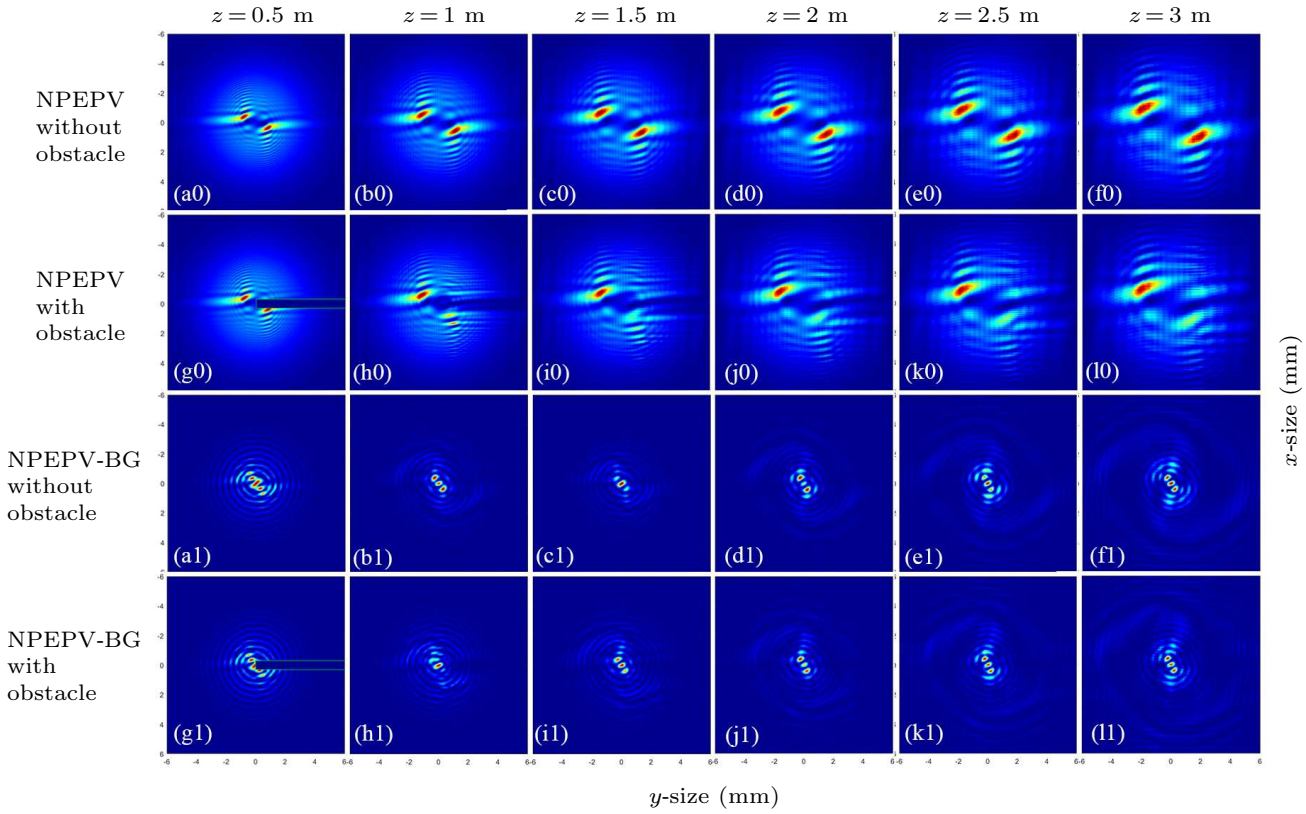


Fig. 6. Intensity evolution of NPEPV beam ($l = 2$, $n = 5$) during the propagation without obstacle (a0)–(f0), and with obstacles (g0)–(l0), at different propagation distances d. Intensity evolution of NPEP-BG beam ($l = 2$, $n = 5$) during the propagation without obstacle (a1)–(f1), and with obstacle (g1)–(l1), at different propagation distances z.

3.4. Focusing characteristic of the NPEP-BG beams

Many laser applications are based on the focusing characteristics of the beam. We focused the NPEP-BG beam by a lens with focal length of $f = 0.2$ m and the other parameters values are the same as those in Subsection 3.1.

The intensity and phase distributions of the focus spot of the NPEPV-BG beam with different TCs and $n = 2$ are shown in Figs. 7(a)–7(d), respectively. From Figs. 7(a)–7(d), we can see that the focal intensity distribution is a structure with multiple rings around a center, and the central intensity increases gradually with the increase of TCs. There is one ring with the strongest intensity for each TCs, in which the number of side lobes is equal to the number of TCs when l is smaller than 5. While the increase in TC is more than 5, one side lobe in the ring is gradually split into two side lobes in Figs. 7(b) and 7(d), and the relative intensity of the extra lobes would be comparable to that of the original lobes at $l = 15$. The multi side lobes in focus can be used to manipulate multiple particles using one NPEP-BG beam. Regardless of TC, the outer phase distributions still exhibit step changes similar to vortex beams.

The intensity distributions with the change of n when $l = 2$ and $l = 10$ are shown in Figs. 8(a1)–8(c1) and 8(a2)–8(c2), respectively. The center intensity is increased as the n increases, and the ring distributions are weakened correspondingly. The number of side lobes in the strongest ring is related to the value of l and independent of the n.

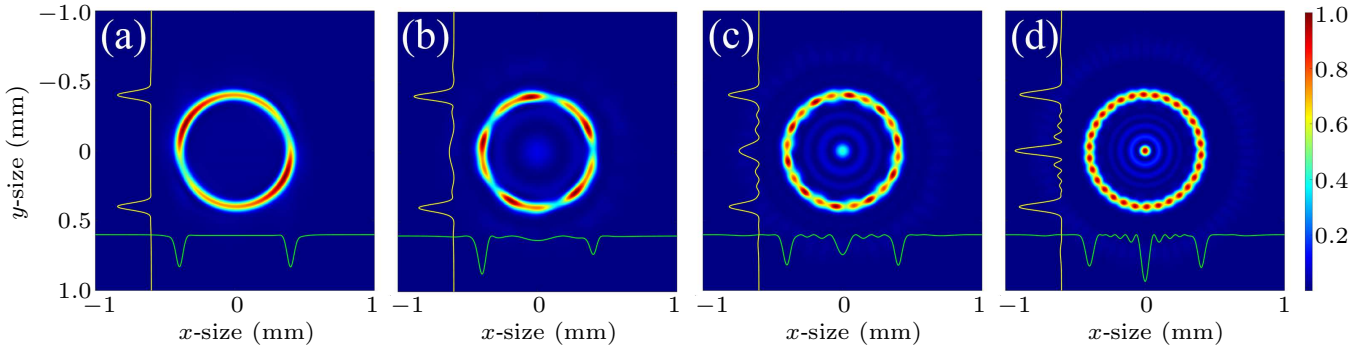


Fig. 7. Intensity (in units of arb. units) of the focal spot of NPEP-BG beam with different TCs and the same power order ($n = 2$) at $z = 0.2$ m. Panels (a)–(d) are the intensities for $l = 2$, $l = 5$, $l = 10$, and $l = 15$ respectively.

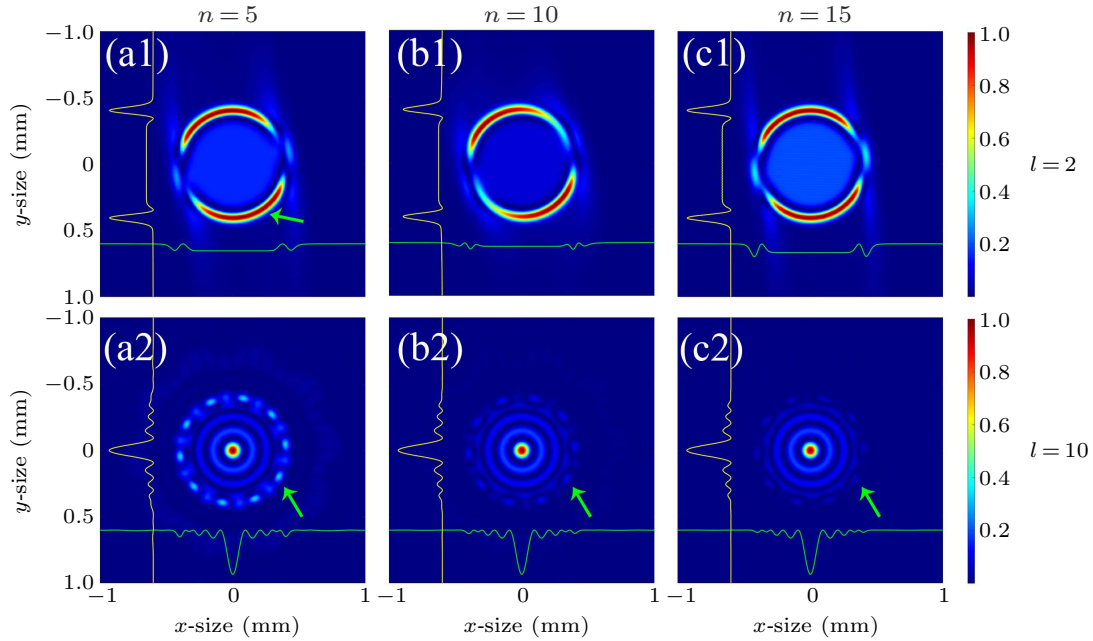


Fig. 8. (a1)–(c1) The intensity (in units of arb. units) distributions for $n = 5$, $n = 10$, and $n = 15$ at $l = 2$. (a2)–(c2) The intensity distribution for $n = 5$, $n = 10$, and $n = 15$ at $l = 10$.

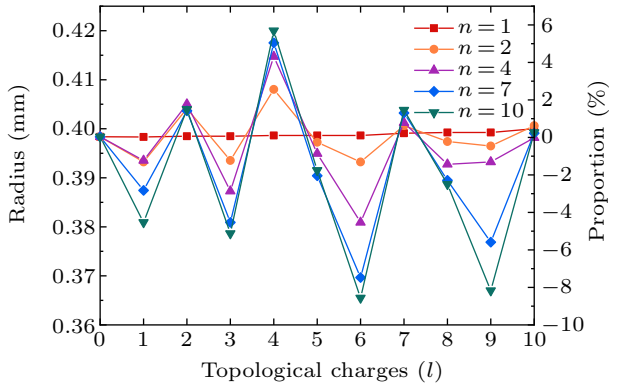


Fig. 9. Left y-axis represents the radius (the length from the discrete side lobes to the center point) of the focal spot with different TCs (l) and power orders (n). The right y-axis represents the proportions of the increasing part of radius compared with radius for $l = 0$, $n = 1$.

Herein, we define the distance from the strongest discrete side-lobe ring (these lobes are marked by green arrows in Fig. 8) to the focus center as the focal radius. Figure 9 shows variation of the focal radius with l from 0 to 10 when $n = 1$, 2, 4, 7, 10, which are represented by the curves of different colors. When $n = 1$, the NPEP-BG beam is equivalent to the BG beam and has the perfect vortex beam characteristics of BG beam in the far field. The focal radius with different values of l and n is represented by curves in Fig. 9. As shown in Fig. 9, the jitter of the curves is relatively gentle when n is small and gradually becomes stronger with the increase of n. Right y-axis in Fig. 9 represents the change ratio of the focal radius with other n and l values compared with focal radius for $l = 0$ and $n = 1$, which is defined as $(y = (r_f - r_{f0})/r_{f0}$, where r_f is the radius for arbitrary l and n, r_{f0} is the radius for $l = 0$, and $l = 1$ with value of 0.398 mm). The result shows that the focal radius of $n > 1$ has only slight changes ($> -8.25\%$ and $< 6\%$) compared with r_{f0}, which means that the focal radius does not obvious increase with the increase of TCs and the focal spot of NPEP-BG has the characteristic similar to perfect vortex beam.

4. Conclusion and perspectives

A novel beam called NPEP-BG, which is a combination of a BG beam and a power exponential phase term, is investigated in this study. The results show that the beam has multiple side lobes in both the near- and far-fields. The number of multiple lobes is related to the topological charge and power exponent. The focus radius of NPEP-BG does not increase with increasing TCs and is close to that of the BG beam with $l = 1$, $n = 1$, which means that the focus of this beam has the characteristics of a perfect vortex beam. The NPEP-BG beam has self-healing characteristics. The NPEP-BG beam has greater potential for application in optical trapping and particle manipulation because of these characteristics.

Acknowledgments

Project supported by the Program of Shanghai Academic/Technology Research Leader (Grant No. 20SR014501), the Strategic Priority Research Program of the Chinese Academy of Sciences (Grant No. XDB1603), and the Youth Innovation Promotion Association of the Chinese Academy of Sciences (Grant No. 2019247).

References

[1] Allen L, Beijersbergen M W and Spreeuw R J C 1992 *Phys. Rev. A* **45** 8185

[2] Wang J, Yang J Y and Fazal I M 2012 *Nat. Photon.* **6** 488
[3] Brunet C, Vaity P and Messaddeq Y 2014 *Opt. Express* **22** 26117
[4] Zhao L, Hao Y and Chen L 2022 *Chin. Opt. Lett.* **20** 020601
[5] Stefan H and Jan W 1994 *Opt. Lett.* **19** 780
[6] Shen Y, Wang X, Xie Z, *et al.* 2019 *Light: Science & Applications* **8** 90
[7] Wang W P, Jiang C and Dong H 2020 *Phys. Rev. Lett.* **125**
[8] Leach J, Yao E and Padgett M J 2004 *New J. Phys.* **6** 71
[9] Lu X, Chen X and Zhang L 2003 *Chin. Phys. Lett.* **20** 2155
[10] Ostrovsky A S, Rickenstorff-Parrao C and Arrizon V 2013 *Opt. Lett.* **38** 534
[11] Vaity P and Rusch L 2015 *Opt. Lett.* **40** 597
[12] Chen M, Mazilu M and Arita Y 2013 *Opt. Lett.* **38** 4919
[13] Lao G, Zhang Z and Zhao D 2016 *Opt. Express* **24** 18082
[14] Ma H, Li X, Zhang H, *et al.* 2019 *Opt. Lett.* **44** 1379
[15] Shen D, Wang K and Zhao D 2019 *Opt. Express* **27** 24642
[16] Fan C, Liu Y and Wang X 2018 *J. Opt. Soc. Am. A* **35** 903
[17] Chen X, Wang X and Wang L 2020 *Photon. Res.* **8** 929
[18] Ren Z, Ying C, Fan C and Wu Q 2012 *Chin. Phys. Lett.* **29** 124209
[19] Durnin J, Jr M J and Eberly J H 1987 *Phys. Rev. Lett.* **58** 1499
[20] Indebetouw G 1989 *J. Opt. Soc. Am. A* **6** 150
[21] Davis J A, Carcole E and Cottrell D M 1996 *Appl. Opt.* **35** 593
[22] Wang J 2016 *Photon. Res.* **4** B14
[23] Khonina S N, Kazanskiy N L and Karpeev S V 2020 *Micromachines* **11** 997
[24] Bai Y, Lv H and Fu X 2022 *Chin. Opt. Lett.* **20** 012601